Materials and Design 194 (2020) 108876

Contents lists available at ScienceDirect

Materials and Design

journal homepage: www.elsevier.com/locate/matdes

Making Fe-Si-B amorphous powders as an effective catalyst for dye degradation by high-energy ultrasonic vibration

Zhuwei Lv [a], Yuqiang Yan [b,1], Chenchen Yuan [a,c,*], Bo Huang [d], Can Yang [b], Jiang Ma [b,**], Junqiang Wang [e], Lishan Huo [f], Zhiqiang Cui [a], Xunli Wang [c], Weihua Wang [g], Baolong Shen [a,***]

[a] School of Materials Science and Engineering, Jiangsu Key Laboratory for Advanced Metallic Materials, Southeast University, Nanjing 211189, People's Republic of China
[b] College of Mechatronics and Control Engineering, Shenzhen University, Shenzhen 518060, People's Republic of China
[c] Department of Physics, City University of Hong Kong, Kowloon, Hong Kong, People's Republic of China
[d] Institute of Materials, School of Materials Science and Engineering, Shanghai University, Shanghai 200444, People's Republic of China
[e] Ningbo Institute of Materials Technology & Engineering, Chinese Academy of Sciences, Ningbo, Zhejiang 315201, People's Republic of China
[f] Ningbo Zhongke B Plus New Materials Technology Co., Ltd, Ningbo, 315201 Zhejiang, People's Republic of China
[g] Institute of Physics, Chinese Academy of Sciences, Beijing 100190, People's Republic of China

HIGHLIGHTS

- Industrial $Fe_{78}Si_9B_{13}$ amorphous powders treated by ultrasonic vibration display an excellent degradation performance.
- Structural rejuvenation during ultrasonic vibration supplies plenty of reactive sites with low density and high energy.
- The activation of micro-channels in rejuvenated $Fe_{78}Si_9B_{13}$ particles offers a shortcut for fast mass transfer.
- Ultrasonic vibration reduces the activation energy of degradation in $Fe_{78}Si_9B_{13}$ amorphous powders.

GRAPHICAL ABSTRACT

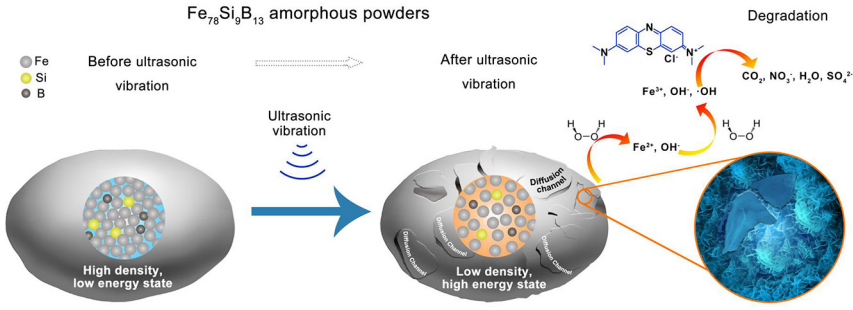

ARTICLE INFO

Article history:
Received 20 February 2020
Received in revised form 6 June 2020
Accepted 8 June 2020
Available online 10 June 2020

Keywords:
Metallic glasses
Ultrasonic vibration
Structural rejuvenation

ABSTRACT

Synthetic dyes have caused serious ecological and environmental threats in our daily lives. Effective and inexpensive dye-degradation methods are desperately perused for decades. In this work, ultrasonic-vibration treatment is found as an effective approach that can dramatically improve the degradation performance of industrial $Fe_{78}Si_9B_{13}$ amorphous powders towards methylene blue. As demonstrated by synchrotron X-ray nano-computed tomography and scanning electron microscope combined with X-ray photoelectron spectroscopy, the micro-channels on the surface or inside of $Fe_{78}Si_9B_{13}$ particles offer a shortcut for fast mass transfer and supply plenty of reactive sites with low density and high energy due to the structural rejuvenation after ultrasonic vibration. It leads to the reduction of the reaction activation energy of degradation under the pseudo-first-order kinetic model and an exceptional decomposition capacity. Our work not only extremely drives down the

* Corresponding author.
** Correspondence to: J. Ma, College of Mechatronics and Control Engineering, Shenzhen University, Shenzhen 518060, People's Republic of China.
*** Correspondence to: B.L. Shen, School of Materials Science and Engineering, Jiangsu Key Laboratory for Advanced metallic Materials, Southeast University, Nanjing 211189, China.
E-mail addresses: yuanchenchenneu@hotmail.com (C. Yuan), majiang@szu.edu.cn (J. Ma), blshen@seu.edu.cn (B. Shen).
[1]Contributes equally with the first author.

https://doi.org/10.1016/j.matdes.2020.108876

Dye degradation

current costs of wastewater treatments, but also provides a promising approach for tuning the effectivity of alloying catalysts *via* manipulating the potential energy state of metallic glasses based on the high-frequency mechanical vibration technique.

1. Introduction

Synthetic dyes, which are widely used in the textile industry, have caused serious ecological and environmental threats due to their toxicity, chemical stability, and potential carcinogenicity [1–4]. In the past decade, numerous effective methods for degrading dyes are conducted to reduce their deleterious impacts, including physical adsorption [5], biodegradation [6], chemical oxidation method such as zero-valent metals [3,7,8]. However, most of the technologies are limited in practical engineering applications because of their inherent drawbacks and high cost. For instance, the activated charcoal adsorption requires secondary treatment because it only collects contaminants *via* a physical process, which results in low efficiency and the potential secondary pollution. Although zero-valent metal such as Fe^0 exhibits low cost and high efficiency, it can be easily oxidized, which causes the degradation capability decays rapidly. In order to overcome those disadvantages, metallic glasses (MGs), *e.g.*, Fe- [9–18], Co- [19], Mg- [20–22], Zr- [23], and Al-based [24] MGs, have been introduced as catalysts for dye decomposition, which normally exhibit much higher degradation capability as compared to the crystalline counterpart owing to their metastable structure at the far-from-equilibrium state, the high residual stress, and the high density of unsaturated sites on the surface of MGs [25].

Among all amorphous alloys, Fe-based amorphous alloys have attracted great attention to dye degradation due to their excellent catalytic degradation performance, superior soft magnetic property, and low cost [9–18]. As a type of commercial Fe-based MGs, $Fe_{78}Si_9B_{13}$ MG has a wide industrial application as the magnetic core of distribution transformers [26,27]. A considerable amount of industrial Fe-Si-B MG wastes are produced due to the replacement of the expired components. As much as we're concerned, it burns with a need to find an effective way to reuse these industrial amorphous alloys.

Some studies indicate that Fe-Si-B MG ribbons prepared in laboratories can degrade synthetic dyes by Fenton/Fenton-like reaction in three steps [28–30]:

$$Fe^0 + H_2O_2 \rightarrow Fe^{2+} + 2OH^- \quad (1)$$

$$Fe^{2+} + H_2O_2 \rightarrow Fe^{3+} + \cdot OH + OH^- \quad (2)$$

$$\cdot OH + \text{organics} \rightarrow \text{products} \quad (3)$$

Fe^0 reacts with H_2O_2 to produce Fe^{2+}. Hydroxyl radicals ($\cdot$OH) produced by the Fenton reaction through the reaction of Fe^{2+} with H_2O_2 are strong oxidants that can decompose organics into small inorganic molecules. In order to further improve the degradation capability, these ribbons are treated by ball-milling into powders. This process can enlarge the specific surface area and stimulate more reactive sites [10,31]. However, the ball-milling is an energy- and time-consuming complicated process, which involves a high vacuum environment to prevent the formation of a surface oxide layer that significantly deteriorates the degradation capability [10,12,19]. These disadvantages hinder the industrial application of ball-milling powders during dye wastewater treatment. Thus, developing effective and time-saving methods to enhance the degradation capability of metallic catalysts is an urgent task.

In this study, we retreat industrial $Fe_{78}Si_9B_{13}$ amorphous powders by ultrasonic vibration considering that high-frequency mechanical vibration can cause residual stress inside the powders, and at the same time increase the energy of amorphous/metastable state in a very short time [32,33], *i.e.* rejuvenation of MGs [34,35]. Both of these factors can decrease the reaction activation energy (ΔE) and enhance decomposition capacity. The degradation capability of industrial $Fe_{78}Si_9B_{13}$ amorphous powders treated by ultrasonic vibration towards methylene blue (MB) was investigated. We show that the ΔE of catalysts rejuvenated by ultrasonic vibration is indeed reduced. As demonstrated by synchrotron X-ray nano-computed tomography (nano-CT), the ultrasonic treatment makes the atomic packing less dense with a high inner stored energy and forms nanoscale cracks. This process provides massive channels for mass transfer with low activation energy and stimulates the exfoliation of the passivation layer during the reaction. In this work, we potentially provide a high-efficiency and almost zero-cost solution for dye wastewater treatment. By using this method, we could also recycle those used/waste Fe-based MG powders/ribbons. Moreover, understanding the structural evolution of glassy systems under ultrasonic vibration is important for seeking high catalytic performance in disordered systems as well as their new applications like electrocatalysis [15,25,36,37].

2. Materials and methods

2.1. Preparation of $Fe_{78}Si_9B_{13}$ powders

The amorphous powders with a nominal composition of $Fe_{78}Si_9B_{13}$ (at. %) were purchased commercially, which were prepared by ball-milling under the atmosphere without the protection of inert gases to simulate the environmental effect induced aging and oxidization of the amorphous powders. Before the degradation experiments, these powders were vibrated by an ultrasonic welding machine (BRANSON 2000×) at the energy of 300–2000 J, the trigger force of the ultrasound is 50 N, the amplitude of 100%, and the working pressure of 500 kPa.

2.2. Characterizations of $Fe_{78}Si_9B_{13}$ powders

The amorphous nature of the $Fe_{78}Si_9B_{13}$ amorphous powders before and after ultrasonic vibration was examined by X-ray diffraction (XRD, Smartlab 3) using Cu K_α radiation with a wavelength of 1.54056 Å (2θ = 20–90°). The surface morphology and elemental distribution of powders before and after degradation were observed by a scanning electron microscope (SEM, QUANTA FEG 450, FEI, Hillsboro, OR, USA) equipped with an energy dispersive X-ray spectrometer (EDS). The SEM acceleration voltage is 10 kV, the working distance is 10.3 mm, and the secondary electron detector is adopted. The EDS adopts the point-sweep mode and the acceleration voltage is 30 kV. The local densities of the powders before and after ultrasonic vibration were detected with nano-CT (Beijing Synchrotron Radiation Facility) with the synchrotron X-ray energy of 8 keV in a chamber of high vacuum at room temperature. The detailed mechanism of detecting the microstructure of materials through synchrotron X-ray nano-CT is illustrated in Ref. [38] and [39]. The size of the voxel in the structure reconstructed by synchrotron X-ray nano-CT is 64.1 × 64.1 × 64.1 nm with the spatial resolution about 100 nm. The electronic structure of elements on the surfaces of powders was evaluated by X-ray photoelectron spectroscopy (XPS, ThermoFisher ESCALAB 250Xi) with a monochromatic Al K_α X-ray source ($h\upsilon$ = 1486.6 eV). The degradation reaction products of $Fe_{78}Si_9B_{13}$ amorphous powders were discovered by Fourier Transform infrared spectroscopy (FTIR, Nicolet iS10 FTIR spectrometer) in

the wavenumber range of 4000–400 cm^{-1}. The empty chamber was measured before proceeding with FTIR experiments as the baseline.

2.3. Dye degradation measurements

250 mL MB solution with a concentration of 100 mg L^{-1} was prepared using deionized water in a 500 mL beaker. Then H_2O_2 was added to adjust the concentration to 1 mM. Using 5% H_2SO_4 and 0.1 M NaOH adjust the initial pH = 3 of the solution if not noted. The temperature of the solution (T = 298 K if not noted) was maintained by using a water bath. Powders (0.5 g L^{-1} for different energy experiments and 0.4 g L^{-1} for the other experiments if not noted) were added as catalysts for the decomposition of MB. The solution was mechanically stirred at a fixed speed of about 350–450 r/min during the degradation process. At the predetermined time intervals, 2.5 mL solution was taken out by a syringe and filtered with a 0.22 mm membrane (PES, Tianjin jinteng experimental equipment co. LTD), and then scanned using a UV–Vis spectrophotometer (Shimadzu UV- 1280) to obtain the absorbance spectrum (190–900 nm) of the solution. At least four degradation experiments were conducted for each reaction condition.

3. Result and discussion

3.1. Degradation performance

UV–Vis spectrophotometry was selected to examine the concentration of MB in the solution treated by the original (0 J) and ultrasonic-vibrated $Fe_{78}Si_9B_{13}$ powders at different time intervals. The amorphous nature of industrial $Fe_{78}Si_9B_{13}$ powders was confirmed by XRD before and after ultrasonic vibration (as shown in Fig. S1). The measurement of MB was based on the intensity of its characteristic absorption peak at 653 nm arising from the chromogenic groups [40], as shown in Fig. 1(a) and (b). An obvious decolorization phenomenon is observed during the Fenton-like reaction by using ultrasonic-vibrated powders with the applied energy of 750 J, while no obvious color change occurs when adding 0 J powders, see the inset of Fig. 1(a) and (b). In order to compare different solutions, the concentration of the MB solution is normalized in Fig. 1(c). It is found that the original industrial powders show poor degradation capability, while the ultrasonic-vibrated powders exhibit a notable degradation of MB solution by the Fenton-like reaction. As the applied energy of ultrasonic vibration is enhanced, the degradation capability of the powder increases gradually. It reaches the highest value at around 500–1000 J and then decreases slightly.

The degradation kinetics after the first 3 min is commonly described by the pseudo-first-order equation as given below [18]:

$$C_t = C_0 \exp(-kt) \tag{4}$$

where k is the reaction rate constant (min^{-1}), t the reaction time (min), C_0 the initial concentration of MB (mg L^{-1}), and C_t the instant concentration of MB (mg L^{-1}) at time t. According to Eq. (4), the reaction rate constant k can be derived by $\ln(C_0/C_t)$ *vs.* t curve. As shown in Fig. 1(d), the experimental data can be successfully fitted by using Eq. (4), where the correlation coefficient R^2 is higher than 97. The corresponding fit parameters are listed in Table S1. With the increase of the applied vibration energy from 0 to 1000 J, k increases from 0 to 0.346 min^{-1}, exhibiting an enhancement of degradation capability of ultrasonic-vibrated powders. With further increasing vibration energy to 2000 J, k slightly decreases to 0.184 min^{-1}.

It is known that the working environment has a significant effect on the degradation capability of catalysts [12,30]. Thus, different conditions including different initial pH, powders dosage, and working temperatures are selected to investigate their effects on the decomposition capability in MB by using 750 J ultrasonic-vibrated powders, see details in Supporting Material Fig. S2. Since the $Fe_{78}Si_9B_{13}$ amorphous powders show the best degradation performance towards MB at pH = 3 [28] with the dosage of 0.4 g L^{-1}, the degradation behavior of original and

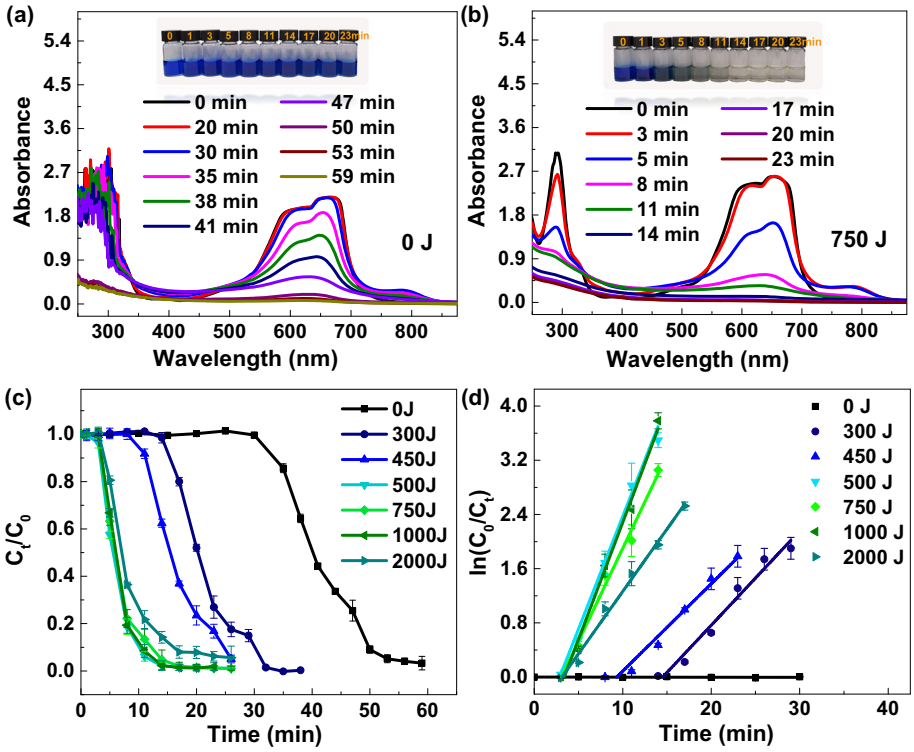

Fig. 1. UV–Vis absorbance spectra of MB solutions during the Fenton-like reaction: (a) original (0 J) and (b) ultrasonic-vibrated (750 J) powders. The insets in (a) and (b) show a visible color change of MB solutions. (c) The normalized concentration change of MB solutions during reactions. (d) The $\ln(C_0/C_t)$ *vs.* time curves for $Fe_{78}Si_9B_{13}$ powders with different applied ultrasonic energy. The solid lines in (d) are the linear fits to the experimental data.

750 J ultrasonic-vibrated $Fe_{78}Si_9B_{13}$ amorphous powders are compared under the following reaction condition: pH = 3, C_{H2O2} = 1 mM, powders dosage = 0.4 g L^{-1}, and C_{MB} = 100 mg L^{-1}.

According to the reaction rate at different temperatures, the thermal activation energy can be derived from the Arrhenius equation [41]:

$$\ln k_T = -\Delta E/(RT) + \ln A \quad (5)$$

As shown in Fig. 2(a) and (b), the ΔE of MB degradations calculated by plotting -ln k_T *vs* 1/*RT* is reduced significantly upon ultrasonic vibration. The ΔE of 0 J powders to degrade MB is 53 ± 3 kJ mol^{-1}, while that of 750 J powders is only 19 ± 1 kJ mol^{-1}. Moreover, the reaction activation energy of the ultrasonic-vibrated sample with the applied energy of 750 J is almost twice lower as compared with the reported value of 34.8 kJ mol^{-1} for $Fe_{78}Si_9B_{13}$ ribbons produced in the laboratory [14].

3.2. Morphologies of the powders

Since the degradation of dye is a surface-mediated process, the changes in the surface morphology of the powders during degradation is examined carefully by SEM. Fig. 3 shows the powder size distribution and the morphology on the surface of $Fe_{78}Si_9B_{13}$ powders. The powder size is estimated to be less than 50 μm. Its distribution is non-uniform. The particles exhibit an irregular-sphere shape with plenty of corrugations, which are the typical characteristics of ball-milling powders [10,42]. Fig. 3(a-f) present SEM images of 0 J powders before and after reactions. There is no significant change on the surface of 0 J powders during degradation. A dense oxide layer is attached to the outside surface of powders with O of 16.45 at. % obtained by EDS (see Table S2), which blocks the mass transport between the solution and the alloying catalyst.

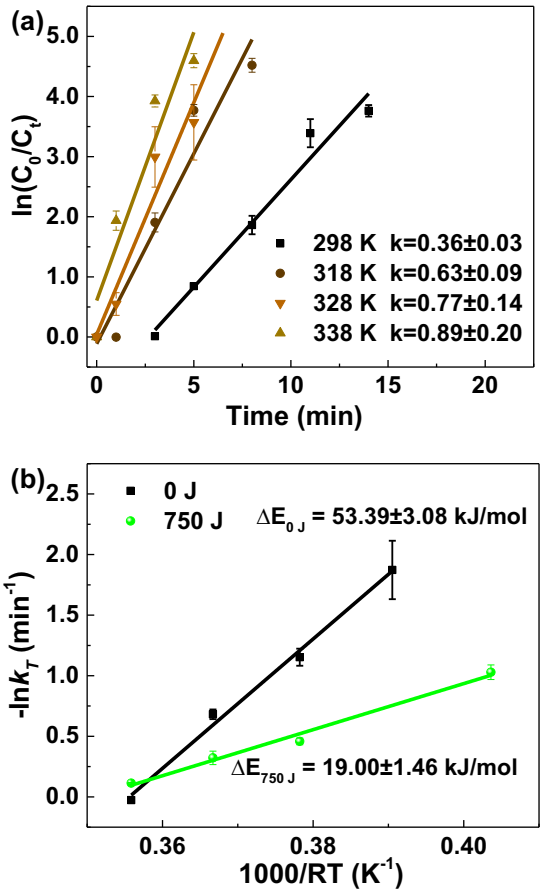

Fig. 2. (a) The ln(C_0/C_t) *vs.* time curves for 750 J powders at different temperatures. (b) The - ln k_T *vs.* 1/*RT* curves for 0 J and 750 J powders.

Fig. 3(g-i) show SEM images of the 0 J and 750 J ultrasonic-vibrated powders before the reaction. A thick oxide film on the surface of the non-ultrasonic-vibration treated powders is also observed in 750 J powders. However, many nanoscale cracks are found after ultrasonic vibration, see the yellow lines in Fig. 3(i). Fig. 3(j-l) show SEM images of the 750 J powders after the reaction. It is seen in Fig. 3(k) that the passivation layer with O of 32.11 at. % (marked as Region A) (Table S2) is falling-off due to the microcracks on the oxide layer. The fresh $Fe_{78}Si_9B_{13}$ underneath the surface then seizes the chance to react with MB. Three-dimension (3D) flowerlike nanostructures, consistent with that reported for the reacted $Fe_{78}Si_9B_{13}$ and FeSiB-based alloys [12], are observed on the surface of reacted 750 J powders (Region B in Fig. 3(l)). The entire structure of the flowerlike architecture is built from several dozens of nanopetals with a smooth surface. Such structure can provide abundant microscopic channels for the diffusion and absorption of the dye molecule, H_2O_2, and ·OH during the decomposition process [43].

Although the passivation film on the surface of powders makes the reaction difficult, a large number of nanoscale cracks generated under ultrasonic-vibration treatment can lead to a fast mass transfer. Besides, the interconnection of cracks during reaction also stimulates the exfoliation of the surface passivation layer. The appearance of microcracks, the generation of 3D nanostructures, and peeling off of the passivation layer during the reaction, thereby accelerate the delivery of substances during degradation.

3.3. Electronic structure of the powders

The chemical effect always has a strong impact on the functionality of MGs [44]. Chemical states of iron can control the generation rate of ·OH, which plays a dominant role in determining the degradation process (Eq. (1–3)), more than the surface/inner morphology [14]. Therefore, XPS is used to comprehend the electronic structural change caused by ultrasonic vibration to understand the underlying mechanism of the improved degradation capability. As shown in Fig. S3, compared with 0 J powders, the XPS spectrum of the 750 J powders shows more O accompanied by the decrease of Fe content (Table S2). It implies that the high energy state of MG powders originating from the structural rejuvenation under ultrasonic vibration [45] may promote the oxidation process, which makes the decomposition easier in virtue of the lower energy barrier of degradation.

3.4. Local densities of the powders

To further explore the structural evolution of powders after ultrasonic vibration, we perform nano-CT experiments to detect the local density of $Fe_{78}Si_9B_{13}$ particles. Fig. 4(a) and (b) show the 3D structure of the typical original and 750 J $Fe_{78}Si_9B_{13}$ amorphous particles with diameters of several microns reconstructed by nano-CT. In these two figures, the red region with a large gray value (*g*) possesses a higher local density as more X-ray is absorbed in the region in the nano-CT experiment [38,39]; the dark blue region with a small *g* possesses a lower local density. It can be seen that a low-density rugged layer appears on the original $Fe_{78}Si_9B_{13}$ particle with its interior denser. After ultrasonic vibration, the rugged layer that stands for the oxide layer on the surface is fragmented and its density becomes smaller, which is consistent with SEM results.

The cross-sections of the reconstructed 3D structure of the $Fe_{78}Si_9B_{13}$ particles before and after ultrasonic vibration are displayed in Fig. 4(c) and (d), respectively, to present the inner structure of the particles more clearly. Apparently, the local density fluctuates inside particles. After ultrasonic vibration, the overall density of the particle including the outer oxide layer seems to become lower, suggesting a higher potential energy state. Interestingly, differ from the untreated particle, a large area in the center of the ultrasonic-vibrated particle

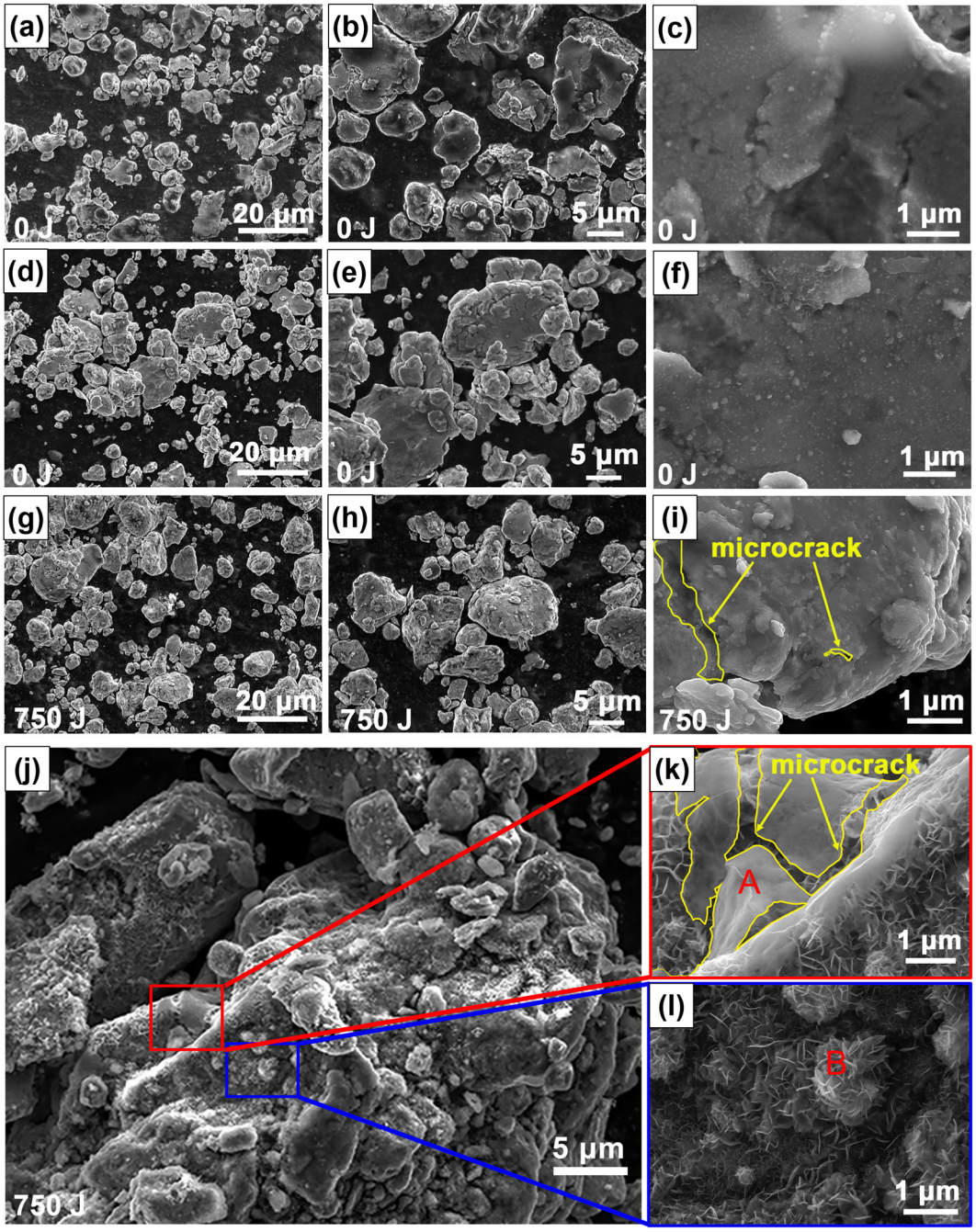

Fig. 3. SEM micrographs of $Fe_{78}Si_9B_{13}$ amorphous powders: 0 J powders (a)-(c) before and (d)-(f) after degradation; 750 J powders before (g)-(i) and after (j-l) degradation.

even possesses a lower packing density than the region near the oxide layer, which could be associated with the high-energy state of atoms. It benefits the propagation of cracks from the surface to the inside, as shown by the white arrows in Fig. 4(d). We find that all $Fe_{78}Si_9B_{13}$ particles show a similar change of the local density after ultrasonic vibration. Thus, the reduction and redistribution of the local density as a result of the structural rejuvenation [34,35] during high-frequency vibration is the main reason that contributes to the high reaction activity of the treated MG powders, which eventually leads to the low ΔE during the degradation process as shown in Fig. 1.

3.5. Pathway of the degradation process

To better understand the process of MB degradation, FTIR analysis was performed, which shows all of the functional groups on the surface of after-degradation $Fe_{78}Si_9B_{13}$ amorphous powders coming from the MB solution or reaction products, see details in Fig. S4. Based on the thorough analyses of the surface/inner morphology and the FTIR spectrum of $Fe_{78}Si_9B_{13}$ powders, the pathway of the degradation reaction of MB can be drawn, as shown in Fig. 5. Metallic iron from $Fe_{78}Si_9B_{13}$ amorphous powders reacts with H_2O_2 in the acidic MB solution and generates the strong oxidizing ·OH. Then, MB molecules undergo redox reaction and are decomposed into small molecules including H_2O, CO_2, NO_3^-, and SO_4^{2-} by cleavage of interlinkage. The reaction pathway of $Fe_{78}Si_9B_{13}$ amorphous powders in this work agrees well with the previously studied Fe-based MGs [9–18]. However, unlike the samples reported in the literature [9–18], $Fe_{78}Si_9B_{13}$ amorphous powders used in this study are industrial powders with a dense oxide film on the surface. The reaction activation energy of industrial powders is about 50% higher than that of the laboratory ribbons produced under the protection of a

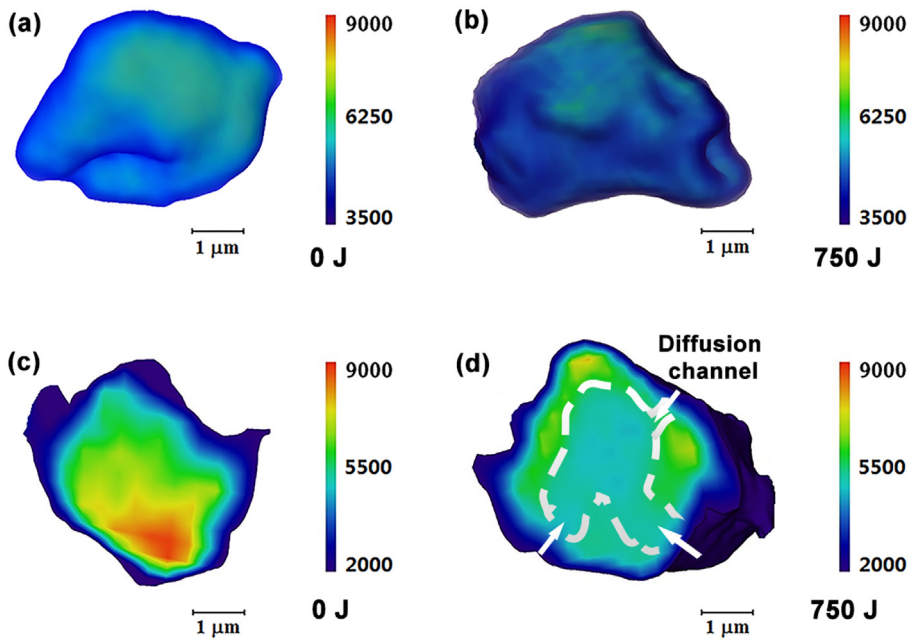

Fig. 4. The structure reconstructed with nano-CT. (a) 0 J and (b) 750 J ultrasonic-vibrated $Fe_{78}Si_9B_{13}$ amorphous particles. The cross-section of the $Fe_{78}Si_9B_{13}$ amorphous particles (c) before and (d) after ultrasonic vibration.

high-purity argon atmosphere [14], see in Fig. 2 (b). As indicated in SEM and nano-CT experiments, ultrasonic vibration can induce the fresh and reactive $Fe_{78}Si_9B_{13}$ interface resulting from the structural rejuvenation [34,35], *i.e.* a low density and high potential energy state, as well as the formation of microcracks/channels with lifting up of passivation film. On the other hand, it has been reported that MGs also undergo a

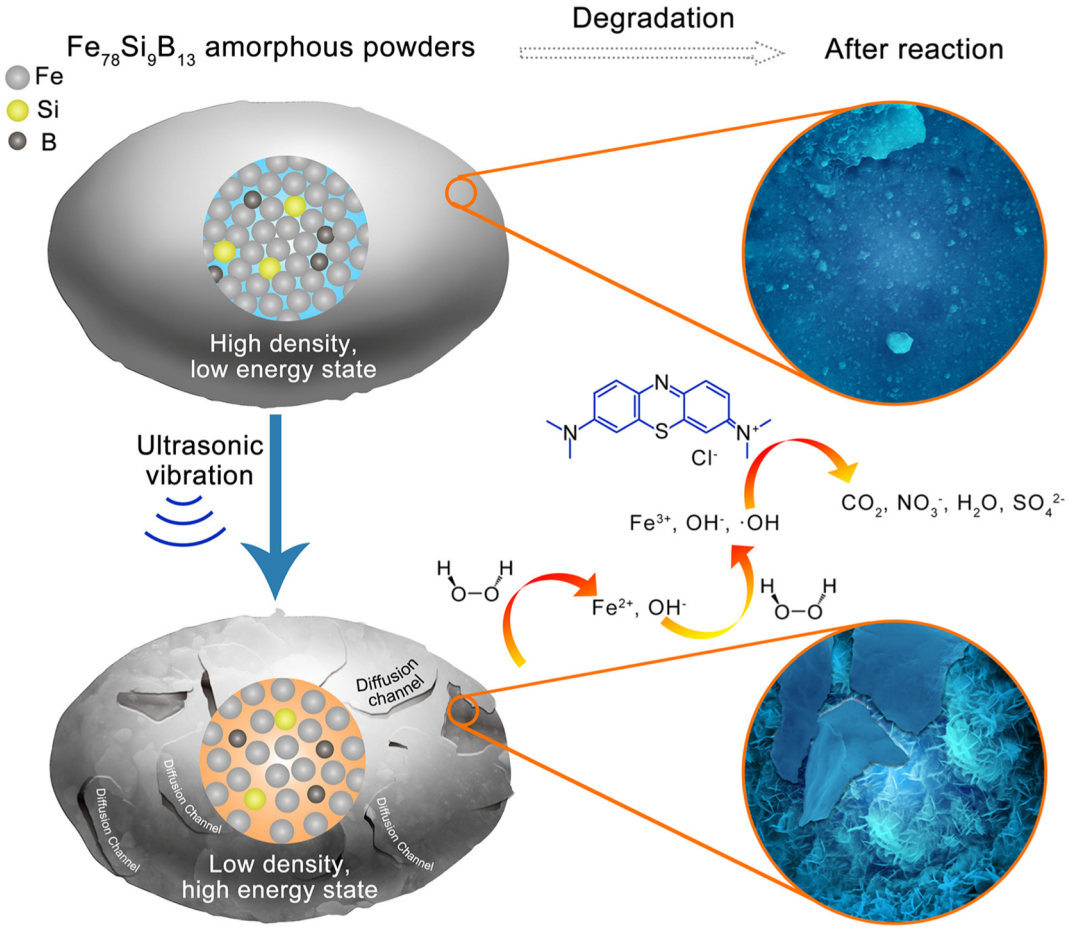

Fig. 5. The pathway of MB degradation by using the original and ultrasonic-vibrated industrial $Fe_{78}Si_9B_{13}$ powders as catalysts.

severe plastic deformation during ultrasonic vibration [46], which results in the large residual stress inside each particle. All of these factors contribute to the highly effective reaction of metallic iron with hydrogen peroxide that occurs on the surface of the loose-packed high-energy powders.

Fig. 6 shows a schematic illustration of the energy landscape in $Fe_{78}Si_9B_{13}$. The energy landscape known as a topographic viewpoint of condensed phases was proposed by Golstein more than 50 years ago [47]. In an N-body material system with a fixed volume, the landscape can be drawn by the manner of a material system. It can provide a convenient framework for interpreting the complex phenomenology [48], for instance, the dynamic behavior under different shear stress [49] or temperatures in glass-forming liquids [50] or proteins [51]. The number of basins, *i.e.* potential energy minima, and the nature of the saddle points separating neighboring basins vary during mechanical deformation [52] or structural transformation [53,54]. As presented in Fig. 6, the activated configurations jump out the saddle point into neighboring basins with a low/high potential energy. The rearrangement of the configuration space during ultrasonic vibration leads to a substantial variation in the depth of basins. Therefore, the potential energy of the glassy system is highly dependent on the vibration energy, see the sketch in the inset of Fig. 6.

When an ultrasound with extremely low energy is applied, structural relaxation of the glass may lead to a series of crystallization behaviors, for instance, the nanocrystalline can be found in the vibrated sample in the work of Pol et al. [55]. Thus, by this technique, we can tune the relaxation process of the glass to obtain different kinds of nanocrystal materials by changing its crystallization route/kinetics. On the other hand, the long-time relaxation also results in the ultrastable state of glass [56], *i.e.*, ideal glass. As reported in both nanoindentation and compression/tension [57,58], a cycling loading within elastic limitation can relax the sample into more stable states like the annealing process [59] and induces hardening either locally or globally. The mechanical vibration, thereby, can be used as an effective method to achieve the ideal state of the glass. More interestingly, when a high-energy vibration is applied, for example in the case of $Fe_{78}Si_9B_{13}$ amorphous powders, a rejuvenation behavior occurs. As illustrated in Fig. 5, the glass transforms from a high atomic-packing density and low-energy state into a metastable state with higher energy and lower density. Such structural rejuvenation due to the injection of the high energy into MGs is also found during the process of severe plastic deformation [60], where more extensive atomic rearrangements accompanied by the creation of excess free volume take place. With further increasing the vibration energy (*e.g.* to higher than 2000 J in this case), the MG sample starts to melt or goes through the glass transition [61]. The devitrification/crystallization then may occur simultaneously, which leads to a slightly worsened degradation efficiency as shown in Fig. 1 (c) and (d). Our studies show that the energy state of glass can be manipulated in a wide potential energy range by using an ultrasonic vibration technique. Thus, we can produce various alloying catalysts with different energy states to satisfy the requirements of most industrial applications. This work demonstrates that the potential energy state of MGs can be easily tuned based on the mechanical vibration technique, which may promote the application of MGs in many fields and also help us better understand the nature of glass.

4. Conclusion

In conclusion, ultrasonic vibration effectively enhances the inner stored energy of MG powders through a structural rejuvenation, which improves the degradation capability by reducing ΔE of the reaction. In addition to the change of the potential energy state, a variety of morphologies of powders' surface were observed, which leads to an accelerating degradation capability as well. The microcracks produced on the surface and inside the powders during the ultrasonic vibration process provide a shortcut for mass transfer and promote the exfoliation of the passivation layer on the surface of the ultrasonic-vibrated powders during the reaction. It breaks through the protection of the passivation film on the surface of industrial powders and supplies "fresh" $Fe_{78}Si_9B_{13}$ with more reaction sites. Meanwhile, 3D flowerlike nanostructure generated during the degradation process also offers massive channels for mass transfer. The pathway of the reaction is sketched based on the above analyses. Our work provides an alternative way for the reuse of wasted Fe-based MGs as an effective catalyst for dye degradation at an extremely low cost. Moreover, a broad picture of controllably tuning the potential energy state of the glass by using the ultrasonic vibration technique has also been drawn, which not only expends industrial applications of MGs but also provides a new perspective on the structural evolution of disordered systems.

Declaration of competing interests

The authors declare that they have no known competing financial interests or personal relationships that could have appeared to influence the work reported in this paper.

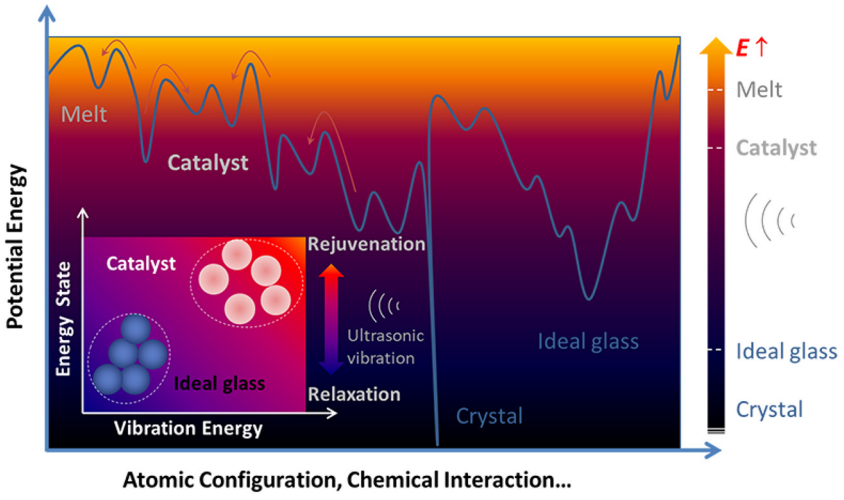

Fig. 6. Schematic illustration of an energy landscape in $Fe_{78}Si_9B_{13}$. The inset shows the changes in the energy state during the structural evolution (relaxation and rejuvenation) upon ultrasonic vibration.

Author contributions

C.C.Y., Z.W.L., and J.M. planned the experimental work. Y.Q.Y. carried out sample preparation and ultrasonic-vibration experiments. L.S.H. help in preparing the powder sample. Z.W.L. carried out the degradation, XRD, XPS, and FTIR experiments. B.H. carried out nano-CT measurements. C.Y. carried out SEM measurements. Z.W.L., C.C.Y., and Z.Q.C. analyzed the experimental data. C.C.Y., Z.W.L, B.H., and J.M. wrote the paper with input and advice from J.Q.W., L.S.H., X.L.W., W.H.W., and B.L.S.

CRediT authorship contribution statement

Zhuwei Lv: Investigation, Formal analysis, Writing - original draft. **Yuqiang Yan:** Resources, Writing - review & editing. **Chenchen Yuan:** Supervision, Conceptualization, Writing - original draft, Writing - review & editing, Funding acquisition. **Bo Huang:** Investigation, Writing - original draft. **Can Yang:** Investigation. **Jiang Ma:** Supervision, Writing - review & editing. **Junqiang Wang:** Writing - review & editing. **Lishan Huo:** Resources. **Zhiqiang Cui:** Data curation. **Xunli Wang:** Writing - review & editing. **Weihua Wang:** Writing - review & editing. **Baolong Shen:** Writing - review & editing, Funding acquisition.

Acknowledgements

Z. W. L. and Y. Q. Y. contributed equally to this work. This work was supported by the National Natural Science Foundation of China (grant numbers 51631003, 51571170, 51901122, and 51601038), the Natural Science Foundation of Jiangsu Province, China (grant number BK20171354). C.C.Y. acknowledges support Jiangsu Key Laboratory for Advanced Metallic Materials (grant number BM2007204). J.M. acknowledges support by the Science and Technology Innovation Commission Shenzhen (grant number JCYJ20170412111216258). B.H. acknowledges support by the Beijing Electron Positron Collider (BEPC) project (grant number 2018-BEPC-PT-001852). X.L.W. acknowledges the support by a grant from the Research Grants Council of the Hong Kong Special Administrative Region, Hong Kong (CityU 11216215), the Croucher Foundation through the CAS-Croucher Foundation Joint Laboratory on Neutron Scattering (CityU 9500034), and the Ministry of Science and Technology of China (grant number 2016YFA0401501). The authors are grateful for the experimental assistance of Wanxia Huang and Qingxi Yuan from National Synchrotron Radiation Lab (NSRL).

Appendix A. Supplementary data

Supplementary data to this article can be found online at https://doi.org/10.1016/j.matdes.2020.108876.

References

[1] J.S. Chang, C. Chou, Y.C. Lin, P.J. Lin, J.Y. Ho, T.L. Ho, Kinetic characteristics of bacterial azo dye decolorization by *Pseudomonas Luteola*, Water Res. 35 (2001) 2841–2850.
[2] B. Manu, S. Chaudhari, Decolorization of indigo and azo dyes in semicontinuous reactors with long hydraulic retention time, Process Biochem. 38 (2003) 1213–1221.
[3] W.X. Zhang, Nanoscale iron particles for environmental remediation: an overview, J. Nanopart. Res. 5 (2003) 323–332.
[4] T. Robinson, G. McMullan, R. Marchant, P. Nigam, Remediation of dyes in textile effluent: a critical review on current treatment technologies with a proposed alternative, Bioresour. Technol. 77 (2001) 247–255.
[5] N.K. Amin, Removal of direct blue-106 dye from aqueous solution using new activated carbons developed from pomegranate peel: adsorption equilibrium and kinetics, J. Hazard. Mater. 165 (2009) 52–62.
[6] S.D. Kalme, G.K. Parshetti, S.U. Jadhav, S.P. Govindwar, Biodegradation of benzidine based dye direct blue-6 by pseudomonas desmolyticum NCIM 2112, Bioresour. Technol. 98 (2007) 1405.
[7] W.A. Arnold, A.L. Roberts, Pathways of chlorinated ethylene and chlorinated acetylene reaction with Zn (0), Environ. Sci. Technol. 33 (1999) 1565.
[8] S. Nam, P.G. Tratnyek, Reduction of azo dyes with zero-valent iron, Wat. Res. 34 (2000) 1837–1845.
[9] C. Zhang, Z. Zhu, H. Zhang, Z. Hu, Rapid reductive degradation of azo dyes by a unique structure of amorphous alloys, Chin. Sci. Bull. 56 (2011) 3988–3992.
[10] J.Q. Wang, Y.H. Liu, M.W. Chen, G.Q. Xie, D.V. Louzguine-Luzgin, A. Inoue, J.H. Perepezko, Rapid degradation of azo dye by Fe-based metallic glass powder, Adv. Funct. Mater. 22 (2012) 2567–2570.
[11] Y. Tang, Y. Shao, N. Chen, K.-F. Yao, Rapid decomposition of direct blue 6 in neutral solution by Fe–B amorphous alloys, RSC Adv. 5 (2015) 6215–6221.
[12] S. Chen, G. Yang, S. Luo, S. Yin, J. Jia, Z. Li, S. Gao, Y. Shao, K. Yao, Unexpected high performance of Fe-based nanocrystallized ribbons for azo dye decomposition, J. Mater. Chem. A 5 (2017) 14230–14240.
[13] X. Qin, Z. Li, Z. Zhu, H. Fu, H. Li, A. Wang, H. Zhang, H. Zhang, Mechanism and kinetics of treatment of acid orange II by aged Fe-Si-B metallic glass powders, J. Mater. Sci. Technol. 33 (2017) 1147–1152.
[14] Q. Wang, M. Chen, P. Lin, Z. Cui, C. Chu, B. Shen, Investigation of FePC amorphous alloys with self-renewing behaviour for highly efficient decolorization of methylene blue, J. Mater. Chem. A 6 (2018) 10686–10699.
[15] S.X. Liang, Z. Jia, Y.J. Liu, W.C. Zhang, W.M. Wang, J. Lu, L.C. Zhang, Compelling rejuvenated catalytic performance in metallic glasses, Adv. Mater. 30 (2018) 1802764.
[16] W. Yang, Q. Wang, W. Li, L. Xue, H. Liu, J. Zhou, J. Mo, B. Shen, A novel thermal-tuning Fe-based amorphous alloy for automatically recycled methylene blue degradation, Mater. Design 161 (2019) 136–146.
[17] J.C. Wang, S.X. Liang, Z. Jia, W.C. Zhang, W.M. Wang, Y.J. Liu, J. Lu, L.C. Zhang, Chemically dealloyed Fe-based metallic glass with void channels-like architecture for highly enhanced peroxymonosulfate activation in catalysis, J. Alloy. Compd. 785 (2019) 642–650.
[18] Z. Jia, Q. Wang, L. Sun, Q. Wang, L.C. Zhang, G. Wu, J.H. Luan, Z.B. Jiao, A. Wang, S.X. Liang, M. Gu, J. Lu, Attractive in situ self-reconstructed hierarchical gradient structure of metallic glass for high efficiency and remarkable stability in catalytic performance, Adv. Funct. Mater. 29 (2019), 1807857.
[19] X.D. Qin, Z.W. Zhu, G. Liu, H.M. Fu, H.W. Zhang, A.M. Wang, H. Li, H.F. Zhang, Ultrafast degradation of azo dyes catalyzed by cobalt-based metallic glass, Sci. Rep. 5 (2015) 18226.
[20] J.Q. Wang, Y.H. Liu, M.W. Chen, D.V. Louzguine-Luzgin, A. Inoue, J.H. Perepezko, Excellent capability in gegrading azo dyes by MgZn-based metallic glass powders, Sci. Rep. 2 (2012) 418.
[21] P. Chen, X. Hu, Y. Qi, X. Wang, Z. Li, L. Zhao, S. Liu, C. Cui, Rapid degradation of azo dyes by melt-spun Mg-Zn-Ca metallic glass in artificial seawater, Metals 7 (2017) 485.
[22] Z. Deng, C. Zhang, L. Liu, Chemically dealloyed MgCuGd metallic glass with enhanced catalytic activity in degradation of phenol, Intermetallics 52 (2014) 9–14.
[23] C. Yang, C. Zhang, W. Xing, L. Liu, 3D printing of Zr-based bulk metallic glasses with complex geometries and enhanced catalytic properties, Intermetallics 94 (2018) 22–28.
[24] P. Wang, J.Q. Wang, H. Li, H. Yang, J. Huo, J. Wang, C. Chang, X. Wang, R.W. Li, G. Wang, Fast decolorization of azo dyes in both alkaline and acidic solutions by Al-based metallic glasses, J. Alloy Compd. 701 (2017) 759–767.
[25] Y.C. Hu, Y.Z. Wang, R. Su, C.R. Cao, F. Li, C.W. Sun, Y. Yang, P.F. Guan, D.W. Ding, Z.L. Wang, W.H. Wang, A highly efficient and self-stabilizing metallic-glass catalyst for electrochemical hydrogen generation, Adv. Mater. 28 (2016) 10293–10297.
[26] R. Hasegawa, Amorphous magnetic materials-a history, J. Magn. Magn. Mater. 100 (1991) 1–12.
[27] F.E. Luborsky, J.J. Becker, J.L. Walter, H.H. Liebermann, Formation and magnetic properties of Fe-B-Si amorphous alloys, IEEE Trans. Magn. 15 (1979) 1146–1149.
[28] X. Wang, Y. Pan, Z. Zhu, J. Wu, Efficient degradation of rhodamine B using Fe-based metallic glass catalyst by Fenton-like process, Chemosphere 117 (2014) 638–643.
[29] S.X. Liang, Z. Jia, W.C. Zhang, X.F. Li, W.M. Wang, H.C. Lin, L.C. Zhang, Ultrafast activation efficiency of three peroxides by Fe78Si9B13 metallic glass under photo-enhanced catalytic oxidation: a comparative study, Appl. Catal. B Environ. 221 (2018) 108–118.
[30] Z. Jia, W.C. Zhang, W.M. Wang, D. Habibi, L.C. Zhang, Amorphous $Fe_{78}Si_9B_{13}$ alloy: an efficient and reusable photo enhanced Fenton like catalyst in degradation of cibacron brilliant red 3B a dye under UV Vis light, Appl. Catal. B Environ. 192 (2016) 46–56.
[31] S. Xie, P. Huang, J.J. Kruzic, X. Zeng, H. Qian, A highly efficient degradation mechanism of methyl orange using Fe-based metallic glass powders, Sci. Rep. 6 (2016), 21947.
[32] K.K.I. Seisakusho, Injection moulding apparatus with an ultrasonic oscillator on the injection nozzle, Japanese Patent (1970) 1–2 JP70006949-B.
[33] W. Presz, T. Kulik, Ultrasonic vibrations as an impulse for glass transition in microforming of bulk metallic glass, Arch. Civ. Mech. Eng. 19 (2018) 100–113.
[34] D.P. Wang, Y. Yang, X.R. Niu, J. Lu, G.N. Yang, W.H. Wang, C.T. Liu, Resonance ultrasonic actuation and local structural rejuvenation in metallic glasses, Phys. Rev. B 95 (2017), 235407.
[35] C. Scalliet, L. Berthier, Rejuvenation and memory effects in a structural glass, Phys. Rev. Lett. 122 (2019), 255502.
[36] J. Wonterghem, S. Mørup, C.J.W. Koch, S.W. Charles, S. Wells, Formation of ultra-fine amorphous alloy particles by reduction in aqueous solution, Nature 322 (1986) 622–623.
[37] M.W. Glasscott, A.D. Pendergast, S. Goines, A.R. Bishop, A.T. Hoang, C. Renault, J.E. Dick, Electrosynthesis of high-entropy metallic glass nanoparticles for designer, multi-functional electrocatalysis, Nat. Commun. 10 (2019) 2650.
[38] Q.X. Yuan, K. Zhang, Y.L. Hong, W.X. Huang, K. Gao, Z.L. Wang, P.P. Zhu, J. Gelb, A. Tkachuk, B. Hornberger, M. Feser, W.B. Yun, Z.Y. Wu, A 30 nm-resolution hard X-ray microscope with X-ray fluorescence mapping capability at BSRF, J. Synchrotron Radiat. 19 (2012) 1021–1028.

[39] B. Huang, T.P. Ge, G.L. Liu, J.H. Luan, Q.F. He, Q.X. Yuan, W.X. Huang, K. Zhang, H.Y. Bai, C.H. Shek, C.T. Liu, Y. Yang, W.H. Wang, Density fluctuations with fractal order in metallic glasses detected by synchrotron X-ray nano-computed tomography, Acta Mater. 155 (2018) 69–79.
[40] Z. Jia, J. Kang, W.C. Zhang, W.M. Wang, C. Yang, H. Sun, D. Habibi, L.C. Zhang, Surface aging behaviour of Fe-based amorphous alloys as catalysts during heterogeneous photo Fenton-like process for water treatment, Appl. Catal. B Environ. 204 (2017) 537–547.
[41] J. Fan, Y. Guo, J. Wang, M. Fan, Rapid Decolorization of azo dye methyl orange in aqueous solution by nanoscale zerovalent iron particles, J. Hazard. Mater. 166 (2009) 904–910.
[42] S.H. Xie, G.Q. Peng, X.M. Tu, H.X. Qian, X.R. Zeng, Fe-based powders prepared by ball-milling with considerable degradation efficiency to methyl orange compared with Fe-based metallic glasses, Acta Metall. Sin. 31 (2018) 1207–1214.
[43] L.S. Zhong, J.S. Hu, H.P. Liang, A.M. Cao, W.G. Song, L.J. Wan, Self-assembled 3D flower-like iron oxide nanostructures and their application in water treatment, Adv. Mater. 18 (2006) 2426–2431.
[44] C.C. Yuan, F. Yang, X.K. Xi, C.L. Shi, D. Holland-Moritz, M.Z. Li, F. Hu, B.L. Shen, X.L. Wang, A. Meyer, W.H. Wang, Impact of hybridization on metallic-glass formation and design, Mater. Today 32 (2020) 26–34.
[45] D.P. Wang, Y. Yang, X.R. Niu, J. Lu, G.N. Yang, W.H. Wang, C.T. Liu, Resonance ultrasonic actuation and local structural rejuvenation in metallic glasses, Phys. Rev. B 95 (2017), 235407.
[46] X. Liang, J. Ma, X.Y. Wu, B. Xu, F. Gong, J.G. Lei, T.J. Peng, R. Cheng, Micro injection of metallic glasses parts under ultrasonic vibration, J. Mater. Sci. Technol. 33 (2017) 703–707.
[47] M. Goldstein, Viscous liquids and the glass transition: a potential energy barrier picture, J. Chem. Phys. 51 (1969) 3728–3739.
[48] F.H. Stillinger, A topographic view of supercooled liquids and glass formation, Science 267 (1995) 1935–1939.
[49] D.L. Malandro, D.J. Lacks, Molecular-level instabilities and enhanced self-diffusion in flowing liquids, Phys. Rev. Lett. 81 (1998) 5576–5579.
[50] S. Sastry, P.G. Debenedetti, F.H. Stillinger, Signatures of distinct dynamical regimes in the energy landscape of a glass-forming liquid, Nature 393 (1998) 554–557.
[51] H. Frauenfelder, S.G. Sligar, P.G. Wolynes, The energy landscapes and motions of proteins, Science 254 (1991) 1598–1603.
[52] D.L. Malandro, D.J. Lacks, Relationships of shear-induced changes in the potential energy landscape to the mechanical properties of ductile glasses, J. Chem. Phys. 110 (1999) 4593–4601.
[53] D.J. Lacks, Localized mechanical instabilities and structural transformations in silica glass under high pressure, Phys. Rev. Lett. 80 (1998) 5385–5388.
[54] S. Lan, Y. Ren, X.Y. Wei, B. Wang, E.P. Gilbert, T. Shibayama, S. Watanabe, M. Ohnuma, X.L. Wang, Hidden amorphous phase and reentrant supercooled liquid in Pd-Ni-P metallic glasses, Nat. Commun. 8 (2017), 14679.
[55] V.G. Pol, A. Gedanken, J. Calderon-Moreno, Deposition of gold nanoparticles on silica spheres: a sonochemical approach, Chem. Mat. 15 (2003) 1111–1118.
[56] H.B. Yu, Y.S. Luo, K. Samwer, Ultrastable metallic glass, Adv. Mater. 25 (2013) 5904–5908.
[57] C.E. Packard, L.M. Witmer, C.A. Schuh, Hardening of a metallic glass during cyclic loading in the elastic range, Appl. Phys. Lett. 92 (17) (2008), 171911.
[58] D.V. Louzguine-Luzgin, V.Y. Zadorozhnyy, S.V. Ketov, Z. Wang, A.A. Tsarkov, A.L. Greer, On room-temperature quasi-elastic mechanical behaviour of bulk metallic glasses, Acta Mater. 129 (2017) 343–351.
[59] C.C. Yuan, J. Ma, X.K. Xi, Understanding the correlation of plastic zone size with characteristic dimple pattern length scale on the fracture surface of a bulk metallic glass, Mater. Sci. Eng. A-Struct. Mater. Prop. Microstruct. Process. 532 (2012) 430–434.
[60] W. Dmowski, Y. Yokoyama, A. Chuang, Y. Ren, M. Umemoto, K. Tsuchiya, A. Inoue, T. Egami, Structural rejuvenation in a bulk metallic glass induced by severe plastic deformation, Acta Mater. 58 (2) (2010) 429–438.
[61] J. Ma, X. Liang, X. Wu, Z. Liu, F. Gong, Sub-second thermoplastic forming of bulk metallic glasses by ultrasonic beating, Sci. Rep. 5 (2015), 17844.